The Astrophysical Journal, 706:925–940, 2009 December 1 doi:10.1088/0004-637X/706/2/925

RUNAWAY STARS, HYPERVELOCITY STARS, AND RADIAL VELOCITY SURVEYS

Benjamin C. Bromley[1], Scott J. Kenyon[2], Warren R. Brown[2], and Margaret J. Geller[2]
[1] Department of Physics, University of Utah, 115 S 1400 E, Rm 201, Salt Lake City, UT 84112, USA; bromley@physics.utah.edu
[2] Smithsonian Astrophysical Observatory, 60 Garden St., Cambridge, MA 02138, USA; skenyon@cfa.harvard.edu, wbrown@cfa.harvard.edu, mgeller@cfa.harvard.edu
Received 2008 December 16; accepted 2009 August 24; published 2009 November 9

ABSTRACT

Runaway stars ejected from the Galactic disk populate the halo of the Milky Way. To predict the spatial and kinematic properties of runaways, we inject stars into a Galactic potential, compute their trajectories through the Galaxy, and derive simulated catalogs for comparison with observations. Runaways have a flattened spatial distribution, with higher velocity stars at Galactic latitudes less than 30°. Due to their shorter stellar lifetimes, massive runaway stars are more concentrated toward the disk than low mass runaways. Bound (unbound) runaways that reach the halo probably originate from distances of 6–12 kpc (10–15 kpc) from the Galactic center, close to the estimated origin of the unbound runaway star HD 271791. Because runaways are brighter and have smaller velocities than hypervelocity stars (HVSs), radial velocity surveys are unlikely to confuse runaway stars with HVSs. We estimate that at most one runaway star contaminates the current sample. We place an upper limit of 2% on the fraction of A-type main-sequence stars ejected as runaways.

Key words: Galaxy: halo – Galaxy: kinematics and dynamics – Galaxy: stellar content – Galaxy: structure – stars: early-type

1. INTRODUCTION

Radial velocity surveys of the Milky Way halo can now reveal rare velocity outliers resulting from dynamical processes throughout the Galaxy. Presently there are three known categories of velocity outliers among main-sequence stars: (1) runaway stars originating in the Galactic disk (Humason & Zwicky 1947); (2) velocity outliers from tidal disruption of dwarf satellites within the halo (Ibata et al. 1994); and (3) hypervelocity stars (HVSs) originating in the Galactic center (Brown et al. 2005). Recent simulations predict the observable spatial and velocity distributions for HVSs (Kenyon et al. 2008) and for remnants of tidal disruption (Abadi et al. 2009). Although runaway stars have been known for a long time, there has been only limited investigation of their observable spatial/velocity distribution throughout the Galaxy.

Here, we simulate the production of runaways and trace their orbits through the Galaxy, concentrating on runaways that reach the halo. We derive the spatial and velocity distributions of runaways as a function of mass and use these results to predict observable quantities for comparison with data from radial velocity surveys. From these results, we estimate the fraction of runaways in surveys of halo stars. We also evaluate the likelihood of runaway star contaminants in targeted surveys for HVSs.

1.1. History and Challenges

First reported by Humason & Zwicky (1947), runaway stars are short-lived stars at unexpectedly large distances and velocities relative to their probable site of origin (Blaauw & Morgan 1954; Greenstein 1957). In the solar neighborhood, roughly 10%–30% of O stars and 5%–10% of B stars are runaways (Gies 1987; Stone 1991). The main population of runaways has a velocity dispersion, 30 km s^{-1}, roughly 3 times larger than the velocity dispersion of non-runaway stars in the Galactic disk. However, several runaways have velocities $\gtrsim$100 km s^{-1} relative to the local standard of rest (e.g., Gies 1987; Stone 1991; Martin 2006) and large distances, $\gtrsim$500 pc, from the Galactic plane (Greenstein & Sargent 1974; Martin 2006). The large velocity dispersion and vertical scale height suggest a dynamical process that ejects runaways from the thin disk into the halo.

Runaways probably originate within star-forming regions in the disk of the Milky Way. Disruption of massive binaries is the likely source of runaways. In the binary supernova mechanism, a main-sequence runaway is ejected when its former companion star explodes as a supernova; subsequent mass loss and the kick velocity from the asymmetric explosion are sufficient to unbind the binary (see Blaauw 1961; Hills 1983). In this scenario, the runaway moves away with roughly the sum of the kick velocity and the orbital velocity of the binary, a velocity physically limited by the orbital velocity at the surface of the stars. In the dynamical ejection mechanism, runaways are ejected in dynamical three- or four-body interactions; the outcome is any combination of single stars and binaries (Poveda et al. 1967; Hoffer 1983; Hut & Bahcall 1983). The maximum ejection velocity from dynamical binary–binary encounters is formally the escape velocity of the most massive star (Leonard 1991).

Understanding whether the proposed formation mechanisms can produce the observed runaway star populations requires high-quality kinematic data and a clear understanding of the dynamics of close binaries and dense star clusters. For large ensembles of runaways, the low binary frequency of runaways favors the dynamical ejection mechanism (Gies & Bolton 1986). However, the predicted kick velocity of supernovae is uncertain (e.g., Burrows et al. 1995; Murphy et al. 2004); if it is large enough, runaways produced by the supernova ejection mechanism will also be single. For individual runaways, it is possible to identify a point of origin by measuring accurate distances, proper motions, and radial velocities (e.g., Hoogerwerf et al. 2001; de Wit et al. 2005; Martin 2006; Heber et al. 2008). For example, using Hipparcos data and accurate radial velocities, Hoogerwerf et al. (2001) (1) associate the runaway star ζ Oph and the pulsar PSR J1932+1059 with a supernova in the Sco OB2 association and (2) confirm that AE

Aur, μ Col, and ι Ori were ejected from the Trapezium cluster in the Orion nebula. Thus, both runaway mechanisms occur in nature.

Existing observational and theoretical results place few constraints on the spatial and velocity distribution of runaways throughout the Milky Way. Because accurate proper motions are often crucial for identifying runaways, known runaways are observed largely in the solar neighborhood (e.g., Conlon et al. 1990; Holmgren et al. 1992; Mitchell et al. 1998; Rolleston et al. 1999; Hoogerwerf et al. 2001; Ramspeck et al. 2001; Magee et al. 2001; Lynn et al. 2004; Martin 2004, 2006). Although some runaways have large distances from the Galactic plane (e.g., Greenstein & Sargent 1974; Heber et al. 2008), few are in the Galactic halo. Numerical simulations currently provide little insight into runaways as probes of the Galactic halo structure. Davies et al. (2002) simulated the distribution of runaways, but only in the context of high-velocity white dwarfs near the Sun. Martin (2006) proposed using runaways to constrain the Galactic potential, but he concluded that known runaways provide few constraints on the large-scale properties of the Galaxy.

1.2. From the Galactic Disk to the Halo

Recent observations of "HVSs" in the halo motivate a broader investigation of the spatial and velocity distribution of runaways. The first HVS is a $3\,M_\odot$ main-sequence star traveling at least twice the escape velocity of the Galaxy at its distance of $\sim$110 kpc (Brown et al. 2005, 2009a). After two other serendipitous discoveries (Hirsch et al. 2005; Edelmann et al. 2005), subsequent targeted searches of the halo yielded a sample of 15 unbound HVSs with Galactic rest-frame velocities of 350–700 km s^{-1} and a similar number of bound HVSs with rest-frame velocities of 275–350 km s^{-1} (Brown et al. 2006a, 2006b, 2007a, 2007b, 2009a). Although the known HVSs are 3–4 $M_\odot$ main-sequence stars roughly uniformly distributed in Galactic latitude, they are not isotropically distributed on the sky (Brown et al. 2009b).

The large space velocity of HVS1 suggests an origin in the Galactic center. As first predicted by Hills (1988), the tidal field of the massive black hole at the Galactic center can unbind a close binary and eject one of the stars at velocities exceeding 2000 km s^{-1}. To distinguish these high-velocity stars from traditional runaway stars, Hills coined the term "hypervelocity star." For typical ejection velocities expected from this mechanism (Hills 1988), we expect a range of velocities similar to those observed in HVSs. Although other dynamical mechanisms involving a black hole can produce HVSs (e.g., Hansen & Milosavljević 2003; Yu & Tremaine 2003; O'Leary & Loeb 2008), the Hills mechanism makes clear predictions for the expected velocity distribution of HVSs ejected from the Galactic center. Kenyon et al. (2008) use these predictions in a numerical simulation of the trajectories of HVSs through the Galaxy. They show that the relative number of bound and unbound HVSs predicted by the Hills mechanism agrees with observations of known HVSs.

Recent observations suggest that runaways can also achieve unbound velocities. The likely unbound star HD 271791 was probably ejected from the disk at 12–16 kpc from the Galactic center (Heber et al. 2008; Przybilla et al. 2008a). Justham et al. (2009) propose that the hot subdwarf US 708, with a heliocentric radial velocity of 708 km s^{-1} (Hirsch et al. 2005), is also a runaway. The apparent overlap in the velocity and spatial distributions of runaways and HVSs suggests that several mechanisms may inject massive main-sequence stars into the halo. The relative contributions of these processes to the structure in the halo remain unknown.

The distribution of runaways and HVSs is also an important issue for large radial velocity surveys. Surveys like RAVE (Zwitter et al. 2008) and SEGUE (Adelman-McCarthy et al. 2008) measure radial velocities for hundreds of thousands of stars in the thin disk, thick disk, and halo. These data will provide fundamental constraints on the escape velocity and total mass of the Milky Way (Smith et al. 2007; Xue et al. 2008; Siebert et al. 2008). Although there are theoretical predictions for observable properties of HVSs in the halo (e.g., Kenyon et al. 2008), there are no predictions for runaway stars in the halo. Thus, the contribution of runaways to velocity outliers in these surveys is unknown.

Here, we use numerical simulations to make a first assay of the spatial and kinematic signature of runaways in large radial velocity surveys. Our focus is on intermediate mass 1.5–6 $M_\odot$ main-sequence stars ejected from the disk into the halo. Intermediate mass stellar lifetimes are 10^8–10^9 yr; thus, these stars formed recently in the disk. The supernova binary disruption scenario requires that the former companion of the runaway was a more massive star with a shorter lifetime. We do not consider massive ($> 6\,M_\odot$) runaways, because they do not live long enough to reach large distances in the halo. We also do not consider low-mass stars because they are intrinsically faint and unobservable at large distances (Kollmeier & Gould 2007; Kenyon et al. 2008).

We construct a model for the spatial and velocity distributions of runaways. We use predicted ejection velocities from the supernova mechanism to eject stars from the exponential disk, and then we track their orbits throughout the Galaxy. In Section 2, we describe the model and the results of our simulations. We apply the simulations to the runaway HD 271791 in Section 3, to HVS surveys in Section 4, and to halo radial velocity surveys in Section 5. We conclude in Section 6.

2. THE SIMULATIONS

The model we construct to explore the global velocity and spatial distribution of runaways in the Milky Way has two components: the gravitational potential of the Galaxy and the velocity distribution of ejected stars. For the Galactic potential, we use the three-component model defined in Kenyon et al. (2008). This disk, bulge, and halo model fits observations of the Galaxy on scales from 5 pc to 100 kpc, and has a circular orbital velocity of 220 km s^{-1} at $r = 8$ kpc (e.g., Hogg et al. 2005).

We consider runaways ejected from an exponential disk with a representative distribution of ejection velocities, explore the propagation of runaways in the Galaxy using a suite of simulations, and examine the resulting distributions in the Galactocentric radius r and radial velocity $v_{\rm rad}$ at the end of the simulation.

2.1. Construction of the Simulations

To generate populations of runaways in the Galaxy, we perform Monte Carlo simulations of 10^6–10^7 stars ejected into three-dimensional orbits from the exponential disk. Each star begins on a circular orbit with velocity $\vec{v}_0(r_{\rm init})$ at some distance $r_{\rm init}$ from the Galactic center in the plane of the Galaxy. The star is ejected at an angle θ_i relative to the orbital velocity vector and an angle b_i relative to the plane of the Galactic disk. For a randomly oriented ejection velocity $\vec{v}_{\rm ej}$, the initial velocity of the ejected star is $\vec{v}_{\rm init} = \vec{v}_0 + \vec{v}_{\rm ej}$. For a star ejected in the direction

of Galactic rotation ($\theta_i \approx 0$), $r_{\rm init}$ becomes the pericenter of its orbit; for a star ejected opposite Galactic rotation ($\theta_i \approx \pi$), $r_{\rm init}$ becomes the apocenter of its orbit.

To follow the trajectories of these ejected stars through the Galaxy, we integrate the equations of motion numerically. In Bromley et al. (2006) and Kenyon et al. (2008), we used a simple leap-frog integrator to track stellar orbits through a one-dimensional Galactic potential. To provide more accurate solutions for the trajectories of runaways in a three-dimensional Galactic potential, here we use an adaptive fourth-order integrator with Richardson extrapolation (e.g., Equations (1)–(3) of Bromley & Kenyon 2006, see also Chapter 15 of Press et al. 1992). Starting at $r_{\rm init}$ with velocity $\vec{v}_{\rm init}$, the code integrates the full three-dimensional orbit through the Galactic potential to track position and velocity as a function of time. We integrate the orbit for a random time t, where t lies between 0 and $t_{\rm ms}$, the main-sequence lifetime of the runaway star. For stars ejected during the supernova explosion of a more massive and much shorter-lived companion star, t is roughly the age of the runaway star.

To motivate choices for the initial conditions of our simulations, we derive the approximate velocities of runaways capable of reaching the outer halo of the Galaxy. Numerical simulations of binary systems disrupted by supernova explosions show that runaways have maximum ejection velocities of ~400 km s^{-1} (Portegies Zwart 2000; Dray et al. 2005). Realistic dynamical ejection models yield similar maximum ejection velocities (Leonard 1993; Fregeau et al. 2004). If the highest velocity runaways are ejected in the direction of Galactic rotation, they receive an additional kick of ≈200 km s^{-1}. Thus, the maximum possible ejection velocity is roughly $v_{\rm ej,max} \approx 600$ km s^{-1}. Unbound HVSs in the outer halo have $v_{\rm rad} \gtrsim 400$ km s^{-1} at $r \approx 70$ kpc (Brown et al. 2009a). To match these properties in our model for the gravitational potential of the Milky Way, runaways must have initial velocities $v_{\rm ej} = 725$ km s^{-1} at $r_{\rm init} = 1$ kpc, $v_{\rm ej} = 550$ km s^{-1} at $r_{\rm init} = 10$ kpc, and $v_{\rm ej} = 500$ km s^{-1} at $r_{\rm init} = 30$ kpc (see Figure 2 of Kenyon et al. 2008). Thus, runaways ejected from $r_{\rm init} \lesssim 5$ kpc cannot reach the outer halo. This conclusion leads us to consider a fiducial set of simulations with $v_{\rm ej} = 400$ km s^{-1} and $r_{\rm init} = 10$ kpc.

Long travel times through the halo constrain our choices for the initial ages and masses of main-sequence runaway stars. Stars with $v_{\rm ej} = 400$ km s^{-1} travel ~40 kpc in ~100 Myr. Thus, stars with main-sequence lifetimes $t_{\rm ms} \gtrsim 100$ Myr and initial masses $m \lesssim 4.5\,M_\odot$ can reach the outer halo (Schaller et al. 1992; Schaerer et al. 1993; Demarque et al. 2004). Stars with $m \approx 4$–$6\,M_\odot$ and $t_{\rm ms} \approx 65$–160 Myr can reach the inner halo. To avoid confusion with indigenous halo stars (see Brown et al. 2006a, 2009a), we focus on main-sequence stars with $m = 1.5$–$6\,M_\odot$ and $t_{\rm ms} = 65$ Myr to 2.9 Gyr (Schaller et al. 1992; Schaerer et al. 1993; Demarque et al. 2004, see also Table 1). These lifetimes are much longer than the lifetimes, $t_{\rm ms} \lesssim$ 10–20 Myr, of their $m \gtrsim 10\,M_\odot$ binary companions that explode as supernovae (Schaller et al. 1992; Schaerer et al. 1993). Thus, we assume for simplicity that runaways have ages of zero when they are ejected from the binary (see also Portegies Zwart 2000).

2.2. Results for a Fiducial Simulation

We first investigate the Galactic distribution of runaways for the fiducial parameters $r_{\rm init} = 10$ kpc, $v_{\rm ej} = 400$ km s^{-1}, and $m = 3\,M_\odot$. Figure 1 shows results for 10^6 runaways; we plot $v_{\rm rad}$ as a function of r. In the upper panel, we color code the points in four intervals of θ_i for stars with $b_i < 30°$. Blue (yellow) points indicate stars ejected with $\theta_i = -\pi/4 \rightarrow \pi/4$ ($\theta_i = 3\pi/4 \rightarrow 5\pi/4$). Cyan and magenta points indicate stars ejected at intermediate angles, $\theta_i = \pm(\pi/4 \rightarrow \pi/2)$ for cyan points and $\theta_i = \pm(\pi/2 \rightarrow 3\pi/4)$ for magenta points. In the lower panel, we color code the points in three intervals of b_i: $b_i < 30°$(cyan), $30° < b_i < 50°$(magenta), and $b_i > 50°$(yellow).

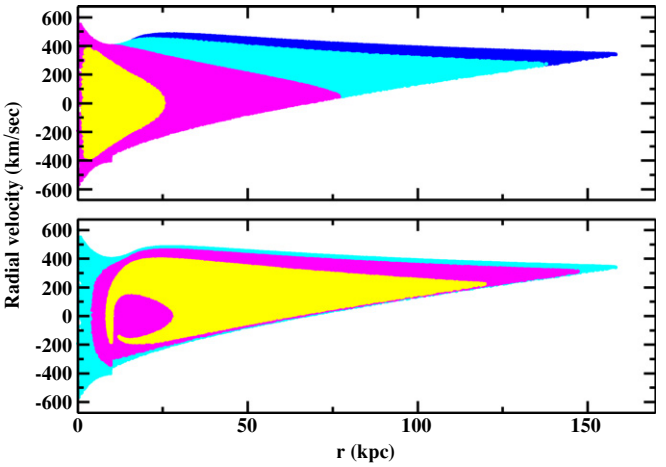

Figure 1. Scatter plots of simulated runaways ejected with $r_{\rm init} = 10$ kpc, $v_{\rm ej} = 400$ km s^{-1}, and $m = 3\,M_\odot$. Each point is a (r, $v_{\rm rad}$) pair derived from a Monte Carlo simulation of 10^6 stars. Upper panel: points ejected into the Galactic disk ($b_i < 30°$) are color-coded according to the ejection angle θ_i relative to the direction of Galactic rotation. Blue (yellow) points indicate stars ejected with $\theta_i = -\pi/4 \rightarrow \pi/4$ ($\theta_i = 3\pi/4 \rightarrow 5\pi/4$). Cyan and magenta points indicate stars ejected at intermediate angles, $\theta_i = \pm(\pi/4 \rightarrow \pi/2)$ for cyan points and $\theta_i = \pm(\pi/2 \rightarrow 3\pi/4)$ for magenta points. Stars ejected along (against) the direction of Galactic rotation reach the largest (smallest) distances in the Galactic halo. Lower panel: points are color-coded according to b_i, the ejection angle relative to the Galactic plane, with $b_i < 30°$ in cyan, $30° < b_i < 50°$ in magenta, and $b_i > 50°$ in yellow. Stars ejected into the plane (halo) reach the largest (smallest) distances from the Galactic center.

The distribution of runaway stars in Figure 1 has several features. In the top panel, stars with the largest initial velocities (blue points) are marginally bound to the Galaxy. Thus, they travel far into the halo, reach a maximum distance $r_{\rm max}$, and then fall back toward the Galactic center. However, the travel time for this orbit, $t \approx \pi r_{\rm max}/v_{\rm init} \sim 1$ Gyr, is longer than the main-sequence lifetime of a $3\,M_\odot$ star, $t_{\rm ms} \approx 350$ Myr. These stars can only be observed on their outward path through the halo and always have positive radial velocities. Thus, the sequence of blue points from (r, $v_{\rm rad}$) = (20, 500) to (160, 340) is an age sequence, with 20–30 Myr-old stars at small r and 300–350 Myr-old stars at the largest r.

Stars ejected opposite to the direction of Galactic rotation (yellow points) have the smallest initial velocities and thus cannot reach large r. These stars live long enough to orbit the Galaxy at least once. Thus, the group of yellow points represents a mixture of young and old stars with a velocity distribution symmetric about zero.

Stars ejected at intermediate angles (cyan and magenta points) fill the (r, $v_{\rm rad}$) space in between the group ejected along or against Galactic rotation. For each group, the sequence from largest $v_{\rm rad}$ to largest r is an age sequence, with younger stars at small r and older stars at large r. Thus, most of the lower envelope of the complete ensemble of points, extending from (r, $v_{\rm rad}$) = (30, −200) to (r, $v_{\rm rad}$) = (160, 340) consists of old stars near the end of their main-sequence lifetimes.

The lower panel of Figure 1 illustrates how the maximum radial velocities decrease with increasing b_i. Stars at high

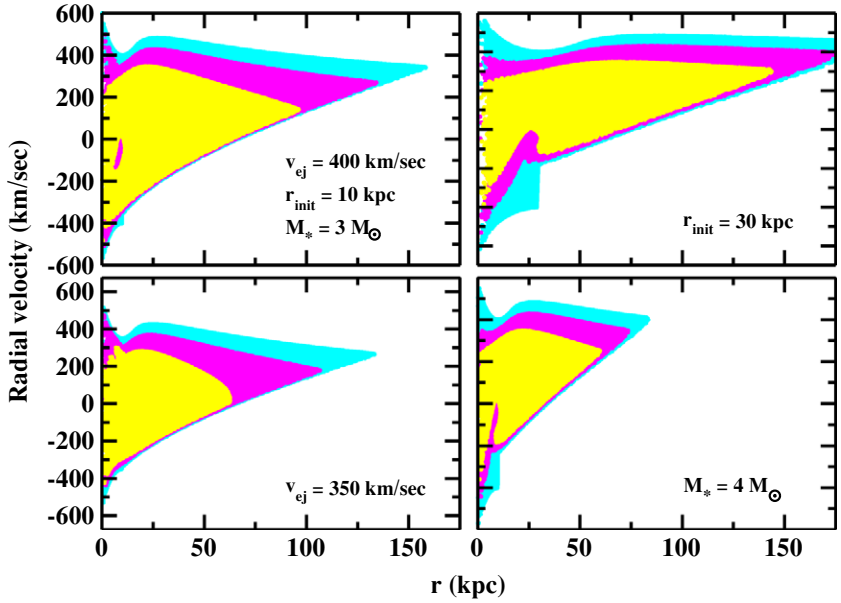

Figure 2. Scatter plots of simulated runaways ejected with the fixed initial radius $r_{\rm init}$, ejection velocity $v_{\rm ej}$, and stellar mass m. Each point is a (r, $v_{\rm rad}$) pair derived from a Monte Carlo simulation of 10^6 stars. In each panel, the colors of the points indicate the Galactic latitude at the end of the simulation; cyan: $b \leqslant 30^\circ$, magenta: $30^\circ < b \leqslant 50^\circ$, and yellow: $b > 50^\circ$. Upper left panel: results of the fiducial simulation with $r_{\rm init} = 10$ kpc, $v_{\rm ej} = 400$ km s^{-1}, and $m = 3\,M_\odot$. Runaways ejected parallel to the plane of the Galactic disk achieve higher $v_{\rm rad}$ at larger r than runaways ejected perpendicular to the disk plane. Upper right panel: results for $r_{\rm init} = 30$ kpc. Runaways ejected at larger $r_{\rm init}$ achieve larger $v_{\rm rad}$ at larger r. Lower left panel: results for $v_{\rm ej} = 350$ km s^{-1}. Runaways ejected with smaller $v_{\rm ej}$ have smaller $v_{\rm rad}$ at all r. Lower right panel: results for $m = 4\,M_\odot$. Smaller main-sequence lifetimes do not allow more massive stars to reach large r.

latitude (yellow points; $b_i \geqslant 50^\circ$) have the smallest velocities, with $v_{\rm rad} \lesssim 400$ km s^{-1} at all r. Stars at intermediate latitudes (magenta points; $30^\circ \leqslant b_i \leqslant 50^\circ$) reach $v_{\rm rad} \lesssim 450$ km s^{-1} at all r; stars at low latitudes (cyan points; $b_i \leqslant 30^\circ$) have the largest final velocities ($v_{\rm rad} \sim 500$ km s^{-1}) and reach the largest final radii, $r = 150$–160 kpc in 350 Myr. The form of the Galactic potential produces this variation. Stars ejected perpendicular to the Galactic disk receive a smaller kick from Galactic rotation compared to stars ejected parallel to the disk. Once stars leave the plane of the disk, they also feel the full disk potential. Thus, stars ejected perpendicular to the disk have smaller initial radial velocities and decelerate faster than stars ejected parallel to the disk.

To show how the results depend on each input parameter, Figure 2 plots the velocity distributions for simulations where we vary each of the three fiducial parameters separately and hold the other two fixed. Here, we color code the points with their final galactic latitude. Instead of illustrating relative densities, our intent in this figure is to show changes in the shape of the distributions of $v_{\rm rad}$ and r as functions of the various input parameters and b_f, the Galactic latitude of stars at the end of the simulation. The upper left panel of Figure 2 repeats the distribution of points in the lower panel of Figure 1 with a different color coding. Here, the variation of $v_{\rm rad}$ and $r_{\rm max}$ with final latitude is much more pronounced than the variation with ejection angle.

The predicted distributions clearly depend on $r_{\rm init}$ and $v_{\rm init}$ (upper right and lower left panels of Figure 2). Stars ejected at small r have to climb out of a deeper potential well than stars ejected at large r. At fixed $v_{\rm ej}$, runaways ejected from 30 kpc have larger velocities in the outer halo (maximum $v_{\rm rad} = 500$ km s^{-1}) than stars ejected from 10 kpc (maximum $v_{\rm rad} = 400$ km s^{-1}). Similarly, stars with smaller (larger) ejection velocities maintain smaller (larger) velocities throughout their passage through the Galaxy. Thus, at fixed $r_{\rm init}$, runaways ejected at larger velocities have larger velocities in the outer halo and reach larger distances in the halo.

Finally, stellar lifetimes have a significant impact on the distributions of position and velocity (Figure 2; lower right panel). For fixed initial ejection velocities, stars with longer main-sequence lifetimes travel farther into the halo. Stars with longer lifetimes can reach large distances with smaller initial radial velocities. Thus, lower mass stars have smaller $v_{\rm rad}$ at larger r. For our adopted main-sequence lifetimes, 1.5–4 $M_\odot$ runaway stars ejected from 10 kpc have asymptotic radial velocities

$$v_{\rm rad}(r_{\rm max,10}) \approx 250(M_\star/2\ M_\odot)^{2/3}\ {\rm km\ s^{-1}} \quad (1)$$

at maximum Galactocentric distances

$$r_{\rm max,10} \approx 400(M_\star/2\ M_\odot)^{-2.4}\ {\rm kpc}. \quad (2)$$

At 30 kpc, runaways have larger asymptotic radial velocities

$$v_{\rm rad}(r_{\rm max,30}) \approx 400(M_\star/2\ M_\odot)^{1/6}\ {\rm km\ s^{-1}} \quad (3)$$

at maximum Galactocentric distances

$$r_{\rm max,30} \approx 575(M_\star/2\ M_\odot)^{-2.6}\ {\rm kpc}. \quad (4)$$

In both equations for $r_{\rm max}$, the large exponent follows from the mass dependence of the main-sequence lifetime ($t_{\rm ms} \propto M_\star^{-3}$; Schaller et al. 1992; Schaerer et al. 1993; Demarque et al. 2004).

Tables 1 and 2 quantify these generic conclusions for an expanded set of fiducial simulations. For simulations with $r_{\rm init} = 10$ kpc, the median velocities in Table 1 show clear trends with stellar mass and r. Only the highest velocity runaways can reach large r; for all stellar masses, the median velocity increases

Table 1
Median Radial Velocities of Runaway Stars [a]

b_f (deg)	Galactocentric Distance r					
	< 20 kpc	20–40 kpc	40–60 kpc	60–80 kpc	80–100 kpc	100–120 kpc
$M_\star = 1.5\ M_\odot$, $t_{ms} = 2.9$ Gyr, $r_{init} = 10$ kpc, $v_{ej} = 400$ km s^{-1}						
0–30	20	15	26	25	31	44
30–50	69	−35	−46	−37	10	23
50–90	−13	94	92	51	34	23
$M_\star = 2\ M_\odot$, $t_{ms} = 1.2$ Gyr, $r_{init} = 10$ kpc, $v_{ej} = 400$ km s^{-1}						
0–30	45	54	83	78	150	170
30–50	110	44	−33	−27	40	58
50–90	10	93	111	62	35	24
$M_\star = 3\ M_\odot$, $t_{ms} = 350$ Myr, $r_{init} = 3$ kpc, $v_{ej} = 400$ km s^{-1}						
0–30	86	122	142	133	150	158
30–50	−36	22	40	37	...	...
50–90	100	33	...	...	...	...
$M_\star = 3\ M_\odot$, $t_{ms} = 350$ Myr, $r_{init} = 10$ kpc, $v_{ej} = 400$ km s^{-1}						
0–30	112	190	240	275	295	304
30–50	222	266	230	210	205	230
50–90	166	190	152	115	130	...
$M_\star = 3\ M_\odot$, $t_{ms} = 350$ Myr, $r_{init} = 30$ kpc, $v_{ej} = 400$ km s^{-1}						
0–30	−36	112	314	339	363	384
30–50	−26	165	281	321	330	333
50–90	60	145	226	254	259	258
$M_\star = 3\ M_\odot$, $t_{ms} = 350$ Myr, $r_{init} = 10$ kpc, $v_{ej} = 350$ km s^{-1}						
0–30	90	155	207	228	232	243
30–50	197	191	104	125	155	176
50–90	98	127	74	42	...	...
$M_\star = 4\ M_\odot$, $t_{ms} = 160$ Myr, $r_{init} = 10$ kpc, $v_{ej} = 400$ km s^{-1}						
0–30	223	320	361	382	404	...
30–50	249	308	295	319	...	...
50–90	201	232	221	...	...	...
$M_\star = 5\ M_\odot$, $t_{ms} = 95$ Myr, $r_{init} = 10$ kpc, $v_{ej} = 400$ km s^{-1}						
0–30	254	388	418	...	...	...
30–50	260	335	359	...	...	...
50–90	217	270	301	...	...	...
$M_\star = 6\ M_\odot$, $t_{ms} = 65$ Myr, $r_{init} = 10$ kpc, $v_{ej} = 400$ km s^{-1}						
0–30	271	418	...	...	...	...
30–50	268	351	...	...	...	...
50–90	239	292	...	...	...	...

Note.
[a] Results for fiducial simulations of 10^6 stars with one initial starting radius, stellar mass, and ejection velocity for all stars. Each entry lists the median v_{rad}, measured in the galactocentric reference frame, as a function of r and b_f for stars with the listed initial conditions. For entries without data, simulations with 10^6 trials do not produce stars with these combinations of r and b_f.

with increasing r. Because their main-sequence lifetimes are longer, lower mass stars typically orbit the Galactic center 2–3 times. Thus, median velocities for lower mass stars are closer to zero than those for higher mass stars.

The trends of median radial velocity with b_f depend on r and stellar mass. Stars ejected into the disk have larger initial velocities and always travel farther than stars ejected perpendicular to the disk. Thus, at large r, stars at the smaller galactic latitude have a larger median v_{rad}. Higher mass stars show the largest variation of median v_{rad}. For every 30° increase in b_f, the median v_{rad} declines ∼25–75 km s^{-1} for 1.5–3 $M_\odot$ stars. At small r, 1.5–3 $M_\odot$ stars with $b_f < 30°$ and $b_f > 50°$ were ejected against Galactic rotation; these stars have a range of orbital phases and thus have the median v_{rad} close to zero. At intermediate b_f, there is a mixture of stars ejected opposite to Galactic rotation (which have median v_{rad} close to zero) and stars ejected with Galactic rotation (which have larger median v_{rad}). Thus, the median velocities for $b_f = 30°$–$50°$ are generally large.

The typical radial velocity dispersions of runaway stars also vary consistently with r, b_f, and stellar mass (Table 2). Stars observed at small r are a mix of young stars ejected into the outer Galaxy and older stars orbiting in the inner Galaxy. Thus, these stars have large velocity dispersions for all stellar masses. Because massive stars have shorter lifetimes, they do not travel far from their ejection point and tend to have smaller velocity

Table 2
Radial Velocity Dispersions of Runaway Stars [a]

b_f (deg)	Galactocentric Distance r					
	< 20 kpc	20–40 kpc	40–60 kpc	60–80 kpc	80–100 kpc	100–120 kpc
$M_\star = 1.5\,M_\odot$, $r_{\rm init} = 10$ kpc, $v_{\rm ej}$= 400 km s^{-1}						
0–30	193	204	177	146	140	144
30–50	200	212	190	168	154	135
50–90	184	158	121	85	70	46
$M_\star = 2\,M_\odot$, $r_{\rm init} = 10$ kpc, $v_{\rm ej}$= 400 km s^{-1}						
0–30	192	199	172	172	174	154
30–50	190	220	200	162	134	110
50–90	187	172	133	90	69	46
$M_\star = 3\,M_\odot$, $r_{\rm init} = 3$ kpc, $v_{\rm ej}$= 400 km s^{-1}						
0–30	179	171	108	64	30	4
30–50	206	134	72	27	...	...
50–90	140	78	...	...	...	...
$M_\star = 3\,M_\odot$, $r_{\rm init} = 10$ kpc, $v_{\rm ej}$= 400 km s^{-1}						
0–30	180	201	157	117	83	54
30–50	155	165	123	84	55	33
50–90	160	136	87	48	23	...
$M_\star = 3\,M_\odot$, $r_{\rm init} = 30$ kpc, $v_{\rm ej}$= 400 km s^{-1}						
0–30	257	180	137	128	109	89
30–50	179	120	104	100	82	61
50–90	101	87	94	77	54	34
$M_\star = 3\,M_\odot$, $r_{\rm init} = 10$ kpc, $v_{\rm ej}$= 350 km s^{-1}						
0–30	165	183	134	92	58	34
30–50	143	148	101	62	32	8
50–90	138	112	61	21	...	...
$M_\star = 4\,M_\odot$, $r_{\rm init} = 10$ kpc, $v_{\rm ej}$= 400 km s^{-1}						
0–30	148	141	85	41	8	...
30–50	124	108	58	27	...	...
50–90	111	83	36	...	...	...
$M_\star = 5\,M_\odot$, $r_{\rm init} = 10$ kpc, $v_{\rm ej}$= 400 km s^{-1}						
0–30	130	103	46	...	...	...
30–50	100	74	31	...	...	...
50–90	82	52	10	...	...	...
$M_\star = 6\,M_\odot$, $r_{\rm init} = 10$ kpc, $v_{\rm ej}$= 400 km s^{-1}						
0–30	127	85	...	...	...	...
30–50	88	61	...	...	...	...
50–90	68	35	...	...	...	...

Note.
[a] Results for fiducial simulations with one initial starting radius and ejection velocity for each stellar mass. Each entry lists the one-dimensional radial velocity dispersion as a function of r and b_f for stars with the listed initial conditions. For entries without data, the simulations do not produce stars with these combinations of r and b_f.

dispersions. Stars observed at large r are older stars traveling on extended bound orbits. None of these stars live long enough to fall back into the Galaxy. Thus, all have large, positive $v_{\rm rad}$, and small velocity dispersions.

2.3. Results for a Galactic Distribution of Runaways

We now consider a simulation for a complete ensemble of runaways ejected from the full Galactic disk. To make this simulation, we adopt probability functions to assign $r_{\rm init}$ and $v_{\rm ej}$ for each runaway star, integrate the orbit through the Galaxy, and derive the radial velocity $v_{\rm rad}$ and position r for each runaway at a random time t in its orbit. Our approach differs from that of Davies et al. (2002), who simulated runaways ejected uniformly from $1 < r < 10$ kpc.

For the initial distribution of $r_{\rm init}$, we assume that stars are ejected from an exponential disk with a radial scale length of 2.4 kpc (Siegel et al. 2002). We adopt an inner radius of 3 kpc and an outer radius of 30 kpc (Brand & Wouterloot 2007). Thus, the probability distribution for $r_{\rm init}$ is

$$p(r_{\rm init}) \propto r_{\rm init} e^{-r_{\rm init}/2.4\,{\rm kpc}}. \quad (5)$$

Runaways ejected from $r_{\rm init} < 3$ kpc cannot reach the outer halo. Runaways ejected from $r_{\rm init} > 30$ kpc are too rare to make a significant impact on the derived distribution of (r, $v_{\rm rad}$).

For the initial distribution of $v_{\rm ej}$, we adopt results from published analyses of runaways ejected from binary systems disrupted by supernovae. Although dynamical encounters can also produce runaways, there are no published simulations predict-

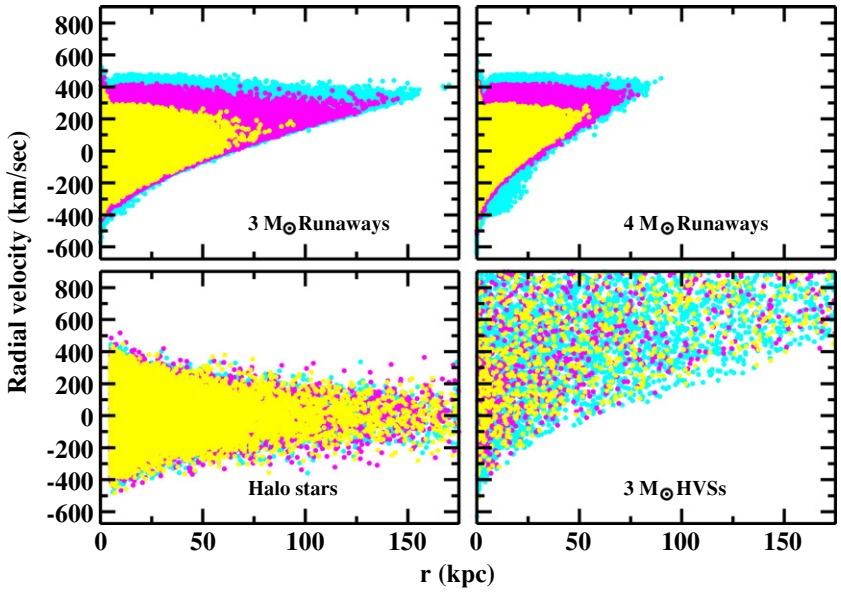

Figure 3. Comparison of (r, $v_{\rm rad}$) diagrams for halo stars, HVSs, and runaways. Stars are color-coded according to their Galactic latitude; cyan: $b_f < 30°$, magenta: $30° < b_f < 50°$, and yellow: $b_f > 50°$. The top panels shows results for $3\,M_\odot$ (left panel) and $4\,M_\odot$ (right panel) runaways ejected from the Galactic disk with probability distributions for $v_{\rm ej}$ (Equation (6)) and for $r_{\rm init}$ (Equation (5)). Longer lived lower mass runaway stars reach larger r than shorter lived more massive runaways. Runaways ejected into the disk achieve larger r than stars ejected perpendicular to the disk. The lower left panel plots the expected velocity distribution of halo stars with a velocity dispersion of 110 km s^{-1} and a $n \propto r^{-3}$ density law. Although nearby halo stars can have large $v_{\rm rad}$, distant runaways have much larger $v_{\rm rad}$ than distant halo stars. The lower right panel shows the expected velocity distribution of HVSs ejected from the Galactic center. At each r, the lower limit to $v_{\rm rad}$ for HVSs follows the predicted lower limit for runaway stars. However, at all r and b_f, HVS have much larger $v_{\rm rad}$ than runaway stars.

ing $p(v_{\rm ej})$ the probability distribution of ejection velocities. For $v_{\rm ej} \sim 20$–400 km s^{-1}, a simple function,

$$p(v_{\rm ej}) \propto e^{-v_{\rm ej}/150\,{\rm km\,s^{-1}}}, \quad (6)$$

provides a reasonable match to the Portegies Zwart (2000) simulations of binary supernova ejections.

We select the Portegies Zwart (2000) ejection velocity distribution function because it is physically well motivated and because a similar distribution function is not available for the dynamical ejection mechanism. Dynamical ejections can attain higher velocities (Leonard & Duncan 1988, 1990; Leonard 1991, 1993); however, the theoretical maximum ejection velocity is not realizable because compact binary interactions are more likely to merge stars than to eject runaways (Fregeau et al. 2004). Moreover, the ejection rate from binary–binary encounters is probably smaller than supernova ejections for intermediate mass stars. Dynamical ejections depend on the joint probability of colliding two binaries within the main-sequence lifetime of the stars (Brown et al. 2009a). Thus, we use the binary-supernova ejection velocity distribution as the representative of the runaway process for 1.5–6 $M_\odot$ stars.

Full-disk simulations of runaways yield many of the same features in the $v_{\rm rad}$–r diagram (Figure 3, top panels). As in Figure 2, the lower envelope of the set of points is defined by an ensemble of old runaways close to the end of their main-sequence lifetimes. Stars ejected into the disk (cyan points) receive the maximum ejection velocity. Thus, these stars have the largest $v_{\rm rad}$ at all r. Stars ejected into the halo (yellow points) have the smallest ejection velocity, the smallest $v_{\rm rad}$ at all r, and the smallest radial extent. More massive stars with shorter $t_{\rm ms}$ do not live long enough to reach large r. Thus, lower mass stars have more extended radial distributions than more massive stars.

The major difference between the fiducial and the full-disk simulations is the variation of the maximum $v_{\rm rad}$ with r. Runaways ejected from the inner disk slowly decelerate as they move from their point of origin. In an ensemble of runaways ejected from a single radius in the inner disk, stars at larger r therefore have smaller $v_{\rm rad}$ than stars at smaller r (upper left panel of Figure 2). However, runaways ejected from the outer disk coast outward at roughly constant $v_{\rm rad}$ (upper right panel of Figure 2). These two features of the evolution combine to produce a roughly constant maximum $v_{\rm rad}$ with r in the top panels of Figure 3. This maximum velocity is independent of stellar mass and is roughly 100 km s^{-1} larger than the maximum ejection velocity.

Tables 3–5 list the median velocities, radial velocity dispersions, and vertical velocity dispersions for the full-disk simulations of 1.5–6 $M_\odot$ stars. For all stellar masses, stars ejected at larger $v_{\rm rad}$ reach larger r. Thus, the median radial velocity increases with r. Because the most distant stars must have roughly the same high ejection velocity to reach large r, these stars have smaller velocity dispersions than the mix of low- and high-velocity runaways at small r. For stars ejected with similar velocities, lower mass stars live longer and can reach larger r. Thus, the median $v_{\rm rad}$ and the velocity dispersions increase with increasing $M_\star$.

The distribution of runaways in the $v_{\rm rad}$–r diagram differs from the distribution of HVSs (Figure 3, lower right panel). The lower envelope of the HVS distribution is identical to the runaway distribution and is composed of stars with ages comparable to their main-sequence lifetimes. However, the distribution of HVSs has three features not observed in runaway stars. The HVS distribution has a core of stars at $r \lesssim 3$ kpc; these stars were ejected from the Galactic center at small velocities ($\lesssim$700 km s^{-1}) and cannot reach large r (Kenyon et al. 2008). Because some HVSs are ejected at very high speeds ($\gtrsim$1200 km s^{-1}), these stars can reach large r with radial velocities much larger than any runaway star. Finally, the velocities of HVSs ejected isotropically from the Galactic center are independent of b. Thus, high-velocity HVSs are

Table 3
Median Radial Velocities of Runaway Stars Ejected from the Galactic Disk[a]

Stellar Mass	Galactocentric Distance r					
	< 20 kpc	20–40 kpc	40–60 kpc	60–80 kpc	80–100 kpc	100–120 kpc
			$b < 30°$			
1.5 $M_\odot$	1	3	7	9	15	16
2 $M_\odot$	2	8	17	29	28	42
3 $M_\odot$	8	23	84	136	188	239
4 $M_\odot$	20	114	239	332	411	...
5 $M_\odot$	53	202	361	...	...	...
6 $M_\odot$	72	246	355	...	...	...
			$30° \leqslant b \leqslant 50°$			
1.5 $M_\odot$	4	10	14	15	16	23
2 $M_\odot$	13	17	16	22	27	38
3 $M_\odot$	50	46	73	121	172	224
4 $M_\odot$	70	115	217	309	...	...
5 $M_\odot$	103	199	334	...	...	...
6 $M_\odot$	144	260	...	...	...	...
			$b > 50°$			
1.5 $M_\odot$	22	48	54	52	68	49
2 $M_\odot$	37	64	70	71	65	48
3 $M_\odot$	72	88	88	108	152	208
4 $M_\odot$	97	127	194	285	...	...
5 $M_\odot$	128	187	287	...	...	...
6 $M_\odot$	169	245	...	...	...	...

Note.
[a] Results for 10^7 stars ejected with velocity $v_{\rm init}$ from $r = r_{\rm init}$ in the Galactic disk. The ejection velocity and position are chosen from probability distributions (Equations (5) and (6)) described in the main text. Each column lists the median $v_{\rm rad}$ for 1.5–6 $M_\odot$ stars with r in the listed range.

Table 4
Radial Velocity Dispersions of Runaway Stars Ejected from the Galactic Disk[a]

Stellar Mass	Galactocentric Distance r					
	< 20 kpc	20–40 kpc	40–60 kpc	60–80 kpc	80–100 kpc	100–120 kpc
			$b < 30°$			
1.5 $M_\odot$	102	127	129	124	116	115
2 $M_\odot$	99	125	126	124	122	112
3 $M_\odot$	94	125	109	86	66	50
4 $M_\odot$	93	102	71	44	32	...
5 $M_\odot$	94	102	53	...	...	...
6 $M_\odot$	104	125	62	...	...	...
			$30° \leqslant b \leqslant 50°$			
1.5 $M_\odot$	121	127	117	116	117	111
2 $M_\odot$	120	127	125	118	106	97
3 $M_\odot$	118	118	96	73	55	40
4 $M_\odot$	102	90	58	34	...	...
5 $M_\odot$	88	74	41	...	...	...
6 $M_\odot$	83	67	...	...	...	...
			$b > 50°$			
1.5 $M_\odot$	121	114	96	84	87	82
2 $M_\odot$	121	110	99	91	88	80
3 $M_\odot$	117	104	79	56	40	25
4 $M_\odot$	103	76	42	15	...	...
5 $M_\odot$	82	54	16	...	...	...
6 $M_\odot$	67	36	...	...	...	...

Note. [a] As in Table 3 for the radial velocity dispersion.

observable at all b. In contrast, high-velocity runaway stars are only observable at low galactic latitude.

The velocity distribution of runaways is also very different from the velocities of halo stars (Figure 3, lower left panel). Halo

Table 5
Vertical Velocity Dispersions of Runaway Stars Ejected from the Galactic Disk[a]

Stellar Mass	Galactocentric Distance r					
	< 20 kpc	20–40 kpc	40–60 kpc	60–80 kpc	80–100 kpc	100–120 kpc
1.5 $M_\odot$	65	60	49	42	36	35
2 $M_\odot$	64	61	51	47	42	37
3 $M_\odot$	67	67	50	41	41	42
4 $M_\odot$	70	62	57	58	52	...
5 $M_\odot$	69	69	68	...	...	...
6 $M_\odot$	71	78	74	...	...	...

Note. [a] As in Table 3 for the velocity dispersion perpendicular to the disk.

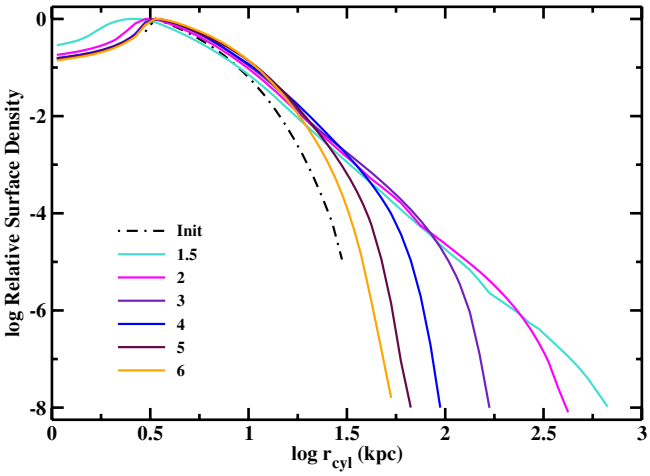

Figure 4. Predicted surface density distributions as a function of cylindrical radius ($r_{\rm cyl}^2 = x_f^2 + y_f^2$) for runaways ejected with a range of velocities (Equation (6)) from an exponential disk (Equation (5)). The dot-dashed black line plots the initial density distribution. The colored lines plot surface density distributions for stars of different masses, as indicated in the legend. For all stars, the density rises slowly from 1–3 kpc, follows a power law ($\Sigma \propto r^{-3.6}$) at intermediate radii, and then falls exponentially at large radii.

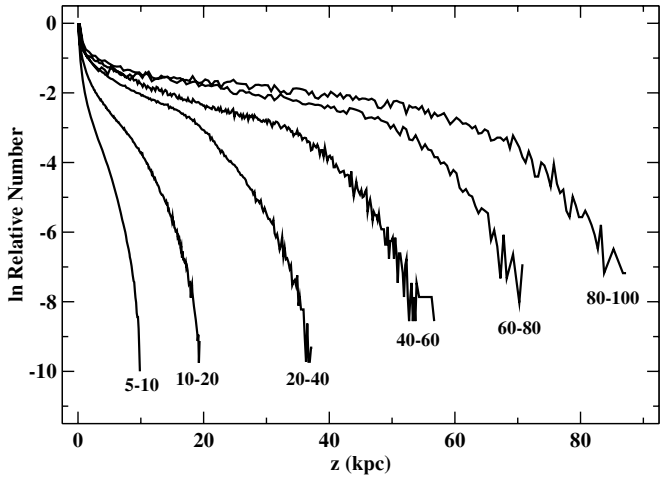

Figure 5. Predicted natural log of the relative number density as a function of z, the height above the disk plane, for 2 $M_\odot$ runaway stars. The curves plot the number density in six cylindrical radius bins, as indicated. In each bin, the density distribution has a central core with a scale height of 300–1000 pc and an extended halo with a scale height of 2–30 kpc. The z scale height of the extended halo increases with increasing cylindrical radius.

stars have a one-dimensional velocity dispersion of roughly 100–110 km s^{-1} (Helmi 2008; Brown et al. 2009a) and a spatial density close to $n \propto r^{-3}$ (Siegel et al. 2002). Thus, the envelope of the halo velocity distribution is symmetric about zero and declines slowly with radius. At large r, there are many halo stars with $v_{\rm rad} \approx 0$. In contrast, there are no intermediate mass HVSs or runaways with $v_{\rm rad} \approx 0$ at large r.

To quantify the differences among runaways, HVSs, and halo stars, we now consider the predicted radial surface density of runaways (Figure 4). Compared to the initial surface density of the Galactic disk (dot-dashed line in Figure 4), runaways are much more radially extended. Runaways ejected against Galactic rotation populate the inner disk ($r \lesssim 3$ kpc). These runaways have a large velocity dispersion at all b (top panels of Figure 3). Runaways ejected at high velocity along Galactic rotation populate the outer disk. These ejections produce a power-law surface density profile, $\Sigma \propto r^{-n}$ with $n = 3.5$–3.6, at intermediate r and an exponential decline at large r. Longer lived lower mass stars have the most extended power-law component. Short-lived massive stars have exponential density profiles more similar to the density profile of the Galactic disk.

Although the density profiles of 1.5–3 $M_\odot$ runaways are extended, they are much steeper than the density profiles of halo stars and HVSs. Fits to observations of halo stars typically yield power-law density profiles with $n \approx 2.7$–3.5 (Helmi 2008, and references therein). Our numerical simulations suggest that low-mass HVSs have a bound component with $n = 3$ and an unbound component with $n = 2$–2.5 (Kenyon et al. 2008; see also Hills 1988). The short, finite lifetimes of massive stars steepen the HVS density profile ($n \gtrsim 3$) at $r \gtrsim 80$ kpc. However, these density profiles remain shallower than the density profiles of runaway stars.

The predicted vertical density distribution also distinguishes runaway stars from halo stars and HVSs (Figure 5). This density distribution has two components. Low-velocity runaways produce a "thick disk" with a vertical scale height of 300–1000 pc. Although more distant runaways have slightly larger "thick disk" scale heights, the scale height is independent of stellar mass. High-velocity runaways lie in an extended disk-shaped halo with a vertical scale height of 2–40 kpc. More distant runaways have much larger vertical scale heights. At $r \lesssim 50$–60 kpc, the scale height of the extended halo is independent of stellar mass (Table 6). At $r \gtrsim 60$ kpc, the vertical scale height depends on stellar mass. Massive stars ($M_\star \gtrsim 4\,M_\odot$) will short main-sequence lifetimes cannot reach large r and thus have no measurable scale height. For stars with longer stellar lifetimes, lower mass stars have smaller scale heights at large r. These smaller scale heights result from low-velocity ejected stars, which have time to reach large r only for the lowest mass main-sequence stars.

Table 6
Vertical Scale Height (in kpc) of Runaway Stars Ejected from the Galactic Disk[a]

Stellar Mass	Galactocentric Distance r					
	< 20 kpc	20–40 kpc	40–60 kpc	60–80 kpc	80–100 kpc	100–120 kpc
1.5 $M_\odot$	1.5	4	9	15	20	25
2 $M_\odot$	1.5	4	10	15	25	30
3 $M_\odot$	1.5	4	10	20	30	40
4 $M_\odot$	1.5	4	15	25	...	...
5 $M_\odot$	2	4	15	...	...	...
6 $M_\odot$	2	4	15	...	...	...

Note. [a] As in Table 3 for the vertical scale height.

Table 7
Median Properties for Unbound Runaway Stars

Stellar Mass	r (kpc)	$v_{\rm rad}$ (km s^{-1})	b_f (deg)
1.5 $M_\odot$	355	210	9
2 $M_\odot$	210	263	9
3 $M_\odot$	82	360	10
4 $M_\odot$	43	400	9
5 $M_\odot$	30	410	8
6 $M_\odot$	23	410	7

The disk-shaped density distribution of the highest velocity runaways differs from the spherically symmetric density distributions of halo stars and HVSs. In our simulations, HVSs ejected from the Galactic center have a spherically symmetric, power-law density distribution with $n \approx 2$–2.5 (Kenyon et al. 2008). Halo stars are also distributed spherically symmetrically and have a steeper radial density profile ($n \approx 2.7$–3.5; Helmi 2008). Because HVSs have a shallower density profile than halo stars, it is easier to identify HVSs at large halo distances than at small halo distances (e.g., Brown et al. 2005; Bromley et al. 2006; Kenyon et al. 2008). The steeper density profiles produced in our runaway star simulations suggest that nearby runaways are easier to identify than distant runaways. We consider this possibility further in Sections 4 and 5.

To conclude this section, we examine several additional properties of simulated runaways in the outer Galaxy. Most runaways with $r \gtrsim 60$ kpc are ejected from inside the solar circle (Figure 6). Although most ejected stars have $r_{\rm init} \approx 3$–6 kpc, small ejection velocities prevent them from reaching $r \gtrsim 60$ kpc (Section 2.1). Because the depth of the Galactic potential is smaller for runaways with $r_{\rm init} \approx 10$–20 kpc, these stars make up a large percentage of stars with $r \gtrsim 60$ kpc (see also Figure 2). In addition, most runaways at large r are low-mass stars with stellar lifetimes long enough to reach the outer Galaxy. With median radial velocities of 10–200 km s^{-1} (Table 3), nearly all of these runaways are bound to the Galaxy. Before reaching the outer galaxy, massive stars ($M_\star \gtrsim 4\,M_\odot$) evolve off the main-sequence and are unobservable at $r \gtrsim 60$ kpc.

Our simulations yield a small fraction—0.07%—of runaways that are *not* bound to the Galaxy. More than half of unbound runaways are ejected from outside the solar circle (double dot-dashed line in Figure 6). Nearly all unbound runaways have low Galactic latitude ($b_f < 30°$; Figure 7 and Table 7). For 1.5–6 $M_\odot$ stars, the shape of the cumulative probability function for b_f is nearly independent of stellar mass. The median of the distribution, however, varies slowly with stellar mass. Our results suggest median Galactic latitude $b_{f,\rm med} = 9°$–$10°$ for 1.5–3 $M_\odot$ stars and $b_{f,\rm med} = 7°$ for 6 $M_\odot$ stars (Table 7).

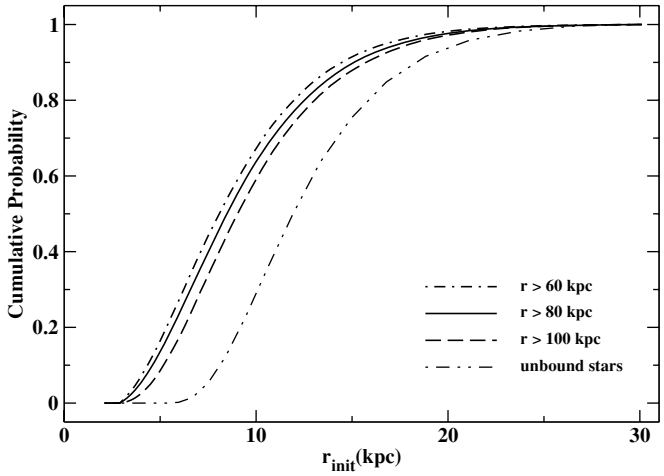

Figure 6. Cumulative probability distributions as a function of the initial disk radius for 2 $M_\odot$ runaway stars. Among runaways that reach final radii $r >$ 60 kpc (dashed line), $r > 80$ kpc (solid line), and $r > 100$ kpc (dot-dashed line), roughly 50% are ejected from inside the solar circle. Among *unbound* runaways (double dot-dashed line), roughly 50% are ejected from $r_{\rm init} \gtrsim 12$ kpc.

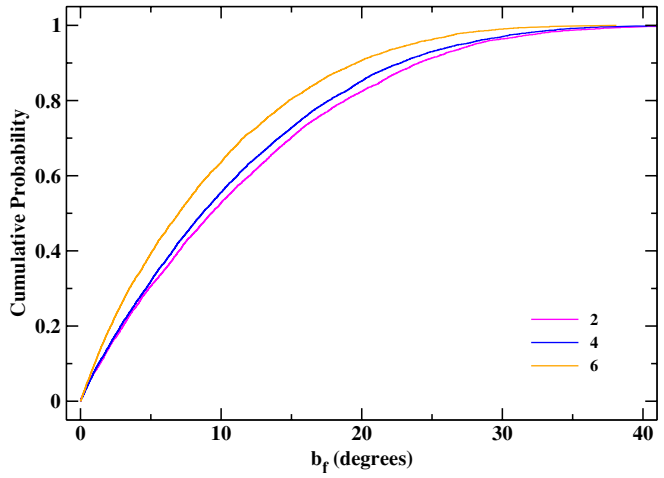

Figure 7. Cumulative probability distributions as a function of the final galactic latitude for unbound runaway stars. The legend indicates the stellar mass for each curve. The median galactic latitude ranges from $b_{f,\rm med} = 7°$ for 6 $M_\odot$ stars to $b_{f,\rm med} = 9°$–$10°$ for 1.5–3 $M_\odot$ stars. All unbound runaways have $b_f < 30°$.

These results for the distribution of b_f contrast with numerical simulations of HVSs, which yield a uniform distribution in b_f (Bromley et al. 2006; Kenyon et al. 2008). In the Hills (1988) ejection mechanism, HVSs are ejected isotropically from the Galactic center. For these stars, the disk is a small perturbation

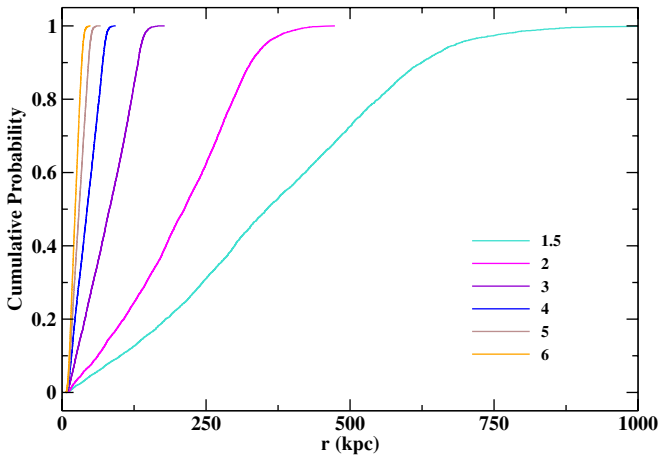

Figure 8. Cumulative probability distributions as a function of the distance for unbound runaway stars. The legend indicates the stellar mass for each curve. Lower mass runaways reach larger r than more massive runaway stars.

on the potential. Thus, simulated HVSs remain uniformly distributed in b_f throughout their path through the Galaxy. For runaway stars, Galactic rotation provides a significant kick to the ejection velocity. Stars ejected with this rotation are more likely to have unbound velocities than other stars (Figures 1–3). Thus, unbound runaways are confined to the plane of the disk.

Although unbound runaways have low b_f independent of $M_\star$, the predicted distances are sensitive to $M_\star$ (Figure 8 and Table 7). The results in Figure 8 show that the cumulative probability of r grows roughly linearly from $r \approx 6$ kpc to $r \approx 0.75 r_{\rm max}$ and then asymptotically approaches 1 at $r \approx r_{\rm max}$. The limiting distance $r_{\rm max}$ of unbound runaways is a strong function of stellar mass. Long-lived low-mass stars travel far into the outer Galaxy ($r_{\rm max} \approx 500$–1000 kpc for $M_\star = 1.5$–$2\,M_\odot$); short-lived high-mass stars rapidly evolve off the main sequence and cannot reach large r ($r_{\rm max} \approx 50$–70 kpc for $M_\star = 5$–$6\,M_\odot$).

2.4. Summary of the Simulations

Our simulations demonstrate how stellar evolution and the Galactic potential combine to influence the dynamical properties of runaway stars ejected from the Galactic disk. Runaways that receive the maximum kick from the binary-supernova mechanism, ≈ 400 km s^{-1}, can travel from the disk into the halo. These stars produce an extended disk-shaped distribution of stars, where the radial and vertical scale lengths are much larger than those of the main stellar disk. The size of this extended disk is very sensitive to stellar mass. Massive stars with short stellar lifetimes are much less extended than long-lived low-mass stars. Because runaways ejected along the direction of Galactic rotation have higher ejection velocities and climb out of a shallower potential well than other runaways, these stars reach larger distances in the outer Galaxy. Although high-velocity runaways appear at all b_f, the fastest unbound runaways are at low galactic latitude, $b_f \lesssim 30^\circ$.

Comparisons of our results with observations of halo stars and simulations of HVSs suggest clear differences between the three populations. Halo stars and HVSs are uniformly distributed in b; runaways are concentrated in the disk. The radial density gradients of halo stars and HVSs are shallower than those of runaways. The $v_{\rm rad}$ distributions of HVSs and runaways are clearly non-Gaussian compared to observations of halo stars; HVSs tend to have larger $v_{\rm rad}$ than runaways. These differences suggest clear observational discriminants of the populations, which we explore in the following sections.

3. APPLICATION TO THE HYPER-RUNAWAY HD 271791

For a first application of our simulations, we consider the runaway B star HD 271791. This B2–3 III star lies well below the Galactic plane ($z \approx -10$ kpc) and has a large heliocentric radial velocity of 442 km s^{-1} (Kilkenny & Stone 1988; Kilkenny & Muller 1989). The observed proper motions suggest a large range in Galactic rest-frame velocity, 530–920 km s^{-1}, and an origin in the outer disk at $r \approx 12$–16 kpc (Heber et al. 2008). Detailed abundance analyses yield a subsolar iron abundance and enhanced abundances of the α-capture nuclei O, Ne, and S (Przybilla et al. 2008a). The subsolar iron abundance supports an origin in the outer Galaxy; the high abundances of α-nuclei imply contamination of the atmosphere from a nearby supernova.

There are two proposals for the origin of HD 271791 as a hyper-runaway star. Przybilla et al. (2008a) suggest that HD 271791 is the secondary of a massive binary disrupted by a supernova. However, the upper limit of the observed rest-frame velocity, $\sim$900 km s^{-1}, is hard to achieve in a close binary system. Thus, Gvaramadze (2009) prefers ejection during a three-body or four-body encounter in the dense core of a massive star cluster.

The large range of allowed rest-frame velocities does not permit a unique interpretation for this star. Here, we first consider the minimum rest-frame velocity of 530 km s^{-1} and note how larger velocities impact our conclusions.

For a rest-frame velocity of 530 km s^{-1}, HD 271791 is a plausible runaway star produced by a supernova explosion in a massive binary system. With a distance $r \approx 21$ kpc from the Galactic center and a height $z \approx -10$ kpc below the Galactic plane (Heber et al. 2008), the star is marginally bound to the Galaxy using the Kenyon et al. (2008) potential model for the Milky Way. The radial velocity is similar to the maximum velocity achieved in our simulations (Figure 3). The galactic latitude of $b \approx -25^\circ$ is marginally consistent with the runaway interpretation. Because the highest velocity runaways are ejected into the disk, only $\approx 5\%$–10% of unbound runaways have $b_f \gtrsim 20^\circ$ (Figure 7). Roughly 30% of unbound runaways are ejected from the apparent origin of HD 271791 at $r \approx 12$–16 kpc (Figure 6). After the ejection, an 11 $M_\odot$ star can reach $z \approx 10$ kpc during its main-sequence lifetime of 20–30 Myr (Table 3; Heber et al. 2008). Thus, the observed spectral type is also consistent with the runaway interpretation.

Larger rest-frame velocities weaken the case for the supernova ejection model. In our simulations, the largest observed rest-frame radial velocity is roughly 100 km s^{-1} larger than the maximum ejection velocity from the binary. An observed rest-frame velocity of $\sim$900 km s^{-1} requires an ejection velocity of 800 km s^{-1}, roughly a factor of 2 larger than the maximum achieved in numerical simulations (Portegies Zwart 2000, see also Przybilla et al.2008). Off-center supernova explosions might enhance the ejection velocity, but factor of 2 increases for a massive star like HD 271791 seem unlikely (Gvaramadze 2009).

Dynamical ejection mechanisms can explain the high rest-frame velocity of HD 271791. Gvaramadze (2009) outlines several mechanisms where the interactions among binary or triple systems produce an ejected star with a velocity of $\lesssim$800 km s^{-1}. To account for the enhanced α-nuclei in the atmosphere, the dynamical encounter(s) in each mechanism must occur close

in time to the supernova explosion of one of the companion stars to HD 271791.

Low probabilities complicate all formation mechanisms for HD 271791 (Brown et al. 2009a). In the Przybilla et al. (2008a) model, a supernova explosion in a 80 $M_\odot$ star produces the high ejection velocity of the secondary. For a Galactic star formation rate of 4 $M_\odot$ yr^{-1} (e.g., Diehl et al. 2006), we expect $\approx 5 \times 10^4$ stars with $M_\star \gtrsim 80\,M_\odot$ during the 25 Myr main-sequence lifetime of HD 271791. Roughly one-third of all O star binaries are twins; for a Salpeter (1955) initial mass function, 5% of the rest have 10–12 $M_\odot$ companions (Kobulnicky & Fryer 2007). Thus, ~1000 massive binaries with 80 $M_\odot$ primary stars have 10–12 $M_\odot$ secondaries. If all supernova ejections in these binaries produce a runaway, we expect $1000 \times 0.08\% \approx 1$ unbound runaway similar to HD 271791 every 25 Myr. Extrapolating the results of our simulations to 11 $M_\odot$ runaways, the joint probability of observing this runaway at $b \approx -25^\circ$ and at the end of its main-sequence lifetime at $r \approx 20$ kpc is ~0.1 (see Table 7). Thus, HD 271791 is an unlikely runaway star.

Brown et al. (2009a) show that the likelihood of observing a hyper-runaway from a dynamical ejection is also very small. Dynamical ejections require interactions between two binary systems composed of massive stars. Thus, the probability of a dynamical ejection is the joint probability of interacting massive pairs of binaries within the stars' main-sequence lifetimes. In an ensemble of dense clusters capable of producing high-velocity ejections, the probability of a 3–4 $M_\odot$ hyper-runaway is $\sim 10^{-5}$. For a Salpeter (1955) initial mass function, 11 $M_\odot$ stars are ~4–5 times less likely than 3–4 $M_\odot$ stars. Thus, dynamical ejections are much less likely than supernova ejections.

An improved proper motion for HD 271791 would place better constraints on formation mechanisms. Current data have large uncertainties, leading to a large range in rest-frame velocity (Heber et al. 2008). Observations with *GAIA*, scheduled for a 2011 launch, would yield a very accurate rest-frame velocity.

4. APPLICATION TO HYPERVELOCITY STARS

We now explore the observational consequences of runaway star distributions for HVS surveys. First, we compare our runaway simulations to numerical simulations of the apparent magnitude and heliocentric radial velocity distributions of HVSs. We then compare our runaway simulations with the HVS observations of Brown et al. Finally, we estimate the possible contribution of runaways to the observed sample of HVSs.

4.1. Predicting Observables from Simulations

We begin by "observing" our numerical simulations for 3 $M_\odot$ runaways and HVSs in a heliocentric reference frame. Known HVSs come mostly from the radial velocity survey of Brown et al. (2006a, 2006b, 2007a, 2007b, 2009a), who target objects with the colors of 3–4 $M_\odot$ stars. Three of the HVSs are confirmed $\simeq$3 $M_\odot$ main-sequence stars (Fuentes et al. 2006; Przybilla et al. 2008b; López-Morales & Bonanos 2008). Girardi et al. (2002, 2004) stellar evolutionary tracks show that a solar metallicity, 3 $M_\odot$ star spends 350 Myr on the main sequence with an average luminosity of $M_g = 0.0$.

Thus, we calculate heliocentric distances and apparent magnitudes for the simulated runaways assuming $M_g = 0.0$ appropriate for a 3 $M_\odot$ star. We assume the that Sun is located at $r = 8$ kpc. We shift the origin of the coordinate system to the Sun and derive heliocentric radial velocities by taking $\vec{v} \cdot \hat{r}$.

Figure 9 plots a heliocentric view of the simulations as a function of Galactic longitude, latitude, and apparent magnitude. The top panels of Figure 9 plot the number distribution of runaways and HVSs. The bottom panels of Figure 9 plot the 50th, 90th, and 99th percentile heliocentric radial velocity of runaways and HVSs.

The spatial concentration of runaways in the disk, discussed in Section 2 above, is evident in Figure 9. Our models predict a greater fraction of runaways in the Galactic center hemisphere $|l| < \pm 90^\circ$ and at low Galactic latitudes $b < 30^\circ$. The fraction of HVSs, on the other hand, is larger than the fraction of runaways in the direction of the Galactic anti-center $l = 180^\circ$ and the Galactic pole $|b| = 90^\circ$. Compared to HVSs, runaways are also apparently bright: 80% of 3 $M_\odot$ runaways are *brighter* than $g = 16$, whereas 85% of 3 $M_\odot$ HVSs are *fainter* than $g = 16$.

Runaways are ejected from a rotating disk. This rotation is apparent in the distribution of heliocentric radial velocities: the median (50th percentile) runaway velocity is negative in the direction of Galactic rotation $0^\circ < l < 180^\circ$ and positive in the opposite direction of Galactic rotation $180^\circ < l < 360^\circ$. Similarly, the latitude dependence of runaway velocities reflects the boost from Galactic rotation at low latitudes. HVSs, on the other hand, are ejected on purely radial trajectories and show no rotation. Median HVS velocities exceed the 99th percentile runaway velocity in every direction on the sky. Fainter stars are faster because only the fastest runaways and HVSs survive to reach the largest distances.

4.2. Comparing Simulations and Observations

We now compare our runaway simulation of 3 $M_\odot$ stars to observations of HVSs. Observed HVSs are significant velocity outliers with minimum radial velocities in the Galactic rest frame > +400 km s^{-1}. The well-defined survey of Brown et al. (2006a, 2006b, 2007a, 2007b, 2009a) samples stars with magnitudes $15 < g < 20.5$ and latitudes $30^\circ \lesssim b < 90^\circ$.

Over the range of magnitude and latitude sampled by the Brown et al. survey, only 0.001% of the simulated 3 $M_\odot$ runaways have velocities > +400 km s^{-1}. These runaways differ in three ways from the observed HVSs. (1) Simulated runaways with radial velocities exceeding 400 km s^{-1} are located at low latitude with median $b = 34^\circ$; observed HVSs are distributed uniformly across Galactic latitude with median $b = 51^\circ$ (Brown et al. 2009b). (2) The > 400 km s^{-1} simulated runaways are bright with median $g = 16$; observed HVSs are faint with median $g = 19$ (Brown et al. 2009a). (3) The fastest simulated runaway with $b > 30^\circ$ has velocity +450 km s^{-1}; observed HVSs have velocities up to +700 km s^{-1}. We conclude that runaways cannot significantly contaminate the HVS samples because the observed distribution of HVSs differs so markedly from that expected for runaways (Figure 9).

We now consider how many runaways with radial velocities exceeding +400 km s^{-1} might be included in the Brown et al. HVS survey. To explore this point, we normalize the number of runaways in our simulation to the total number of 3 $M_\odot$ stars formed in the last 350 Myr. Assuming that the star formation rate in the Galactic disk is 4 $M_\odot$ yr^{-1} (Diehl et al. 2006), $1.4 \times 10^9\,M_\odot$ of stars have formed in the disk in the past 350 Myr. A Salpeter initial mass function, integrated from 0.1 to 100 $M_\odot$ and normalized to $1.4 \times 10^9\,M_\odot$, predicts 1.3×10^7 3–4 $M_\odot$ stars. Assuming that ~1% of all stars are ejected as runaways (see below), we predict ~one 3 $M_\odot$ runaway with +400 km s^{-1} radial velocity in the Brown et al. HVS survey. This prediction is comparable to the analytic estimate in Brown

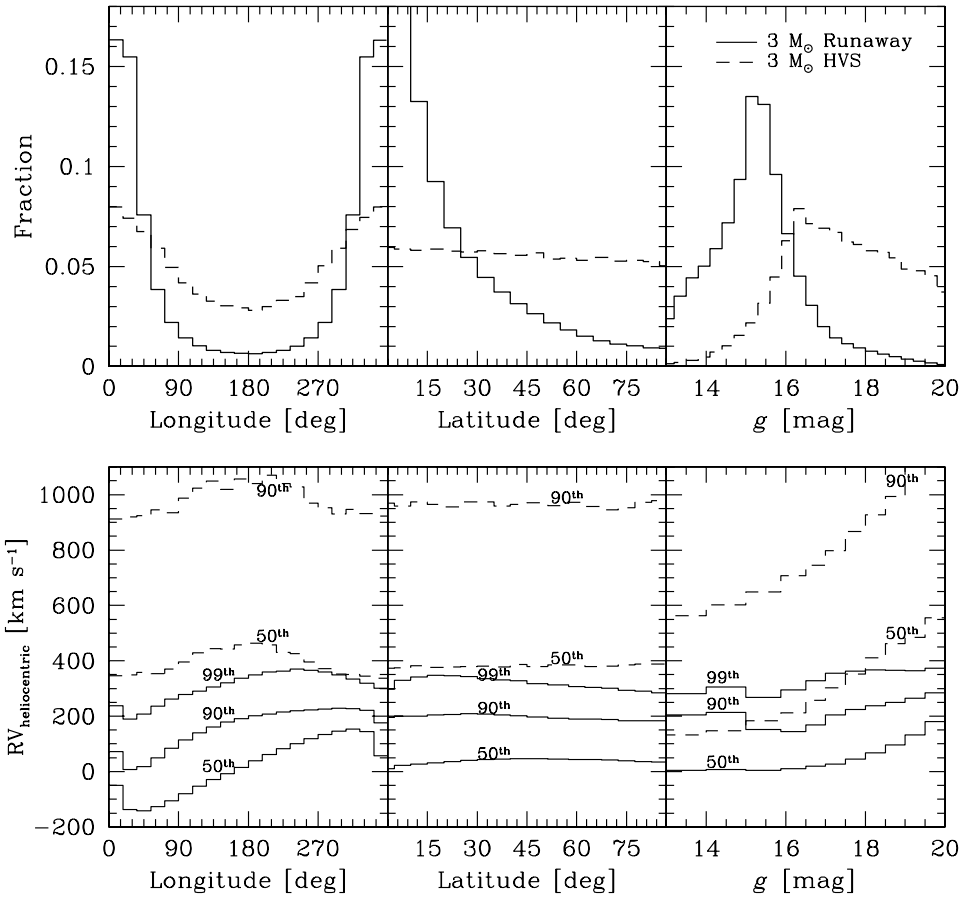

Figure 9. Predicted distributions of runaways and HVSs in a heliocentric reference frame. The top panels plot the number fractions of simulated runaways (solid lines) and HVSs (dashed lines) as a function of Galactic longitude, latitude, and apparent magnitude. Bottom panels plot the 50th, 90th, and 99th percentile heliocentric radial velocities of simulated runaways and HVSs. The spatial and velocity distributions of 3 $M_\odot$ runaways and HVSs are very different: runaways are apparently bright and concentrated to the Galactic plane; HVSs are apparently faint and common in the halo.

et al. (2009a), and suggests that perhaps one of the observed HVSs may be a runaway.

5. APPLICATION TO HALO RADIAL VELOCITY SURVEYS

Large modern photometric and radial velocity surveys open the possibility of global constraints on the number and distribution of runaways. In this section, we consider several examples. We first compare the predictions of our runaway star simulations with the stellar population of the Milky Way derived from color-selected star counts in the Sloan Digital Sky Survey (SDSS). This comparison indicates where future searches for runaways would be most productive. Combined with a Two Micron All Sky Survey (2MASS)-selected spectroscopic survey (Brown et al. 2008), the SDSS counts provide an upper limit on the fraction of disk A main-sequence stars ejected as runaways.

Our numerical simulations demonstrate that runaways reach the inner halo of the Milky Way. Their velocity dispersion is comparable to the halo velocity dispersion; their rotation is comparable with the rotation of the thick disk. Thus, runaways are difficult to identify by their kinematics, but their high metallicities should distinguish them from typical halo stars.

5.1. Comparing Runaways to Star Counts

We begin by comparing our runaway simulations to the observed stellar population of the Milky Way as revealed by star counts in the SDSS Data Release 6 (DR6; Adelman-McCarthy et al. 2008). For this comparison, we select simulations for 1.5 $M_\odot$, 2 $M_\odot$, and 3 $M_\odot$ stars. As before, we "observe" the simulations from a heliocentric reference frame. We calculate apparent magnitudes assuming the 1.5 $M_\odot$, 2 $M_\odot$, and 3 $M_\odot$ runaways have main-sequence luminosities of $M_g = +2.9, +1.5$, and 0.0, respectively (Girardi et al. 2002, 2004).

To compare observed number counts of stars with predictions from our numerical simulations, we consider only runaways that fall in the region of sky imaged by the SDSS DR6. For the stars in the SDSS, we count those stars with colors $0.15 < (g-r)_0 < 0.20$, $-0.15 < (g-r)_0 < -0.05$, and $-0.35 < (g-r)_0 < -0.25$ appropriate for 1.5 $M_\odot$, 2 $M_\odot$, and 3 $M_\odot$ stars, respectively, according to the Girardi et al. (2002, 2004) stellar evolutionary tracks for solar metallicity stars.

Figure 10 plots the resulting number fraction of runaways and SDSS stars as a function of Galactic latitude and apparent magnitude. Over the region surveyed by the SDSS, a larger fraction of runaways are found at low latitudes compared to star counts. This latitude dependence reflects the flattened distribution of runaways compared to the population of halo stars that dominate the star counts. Runaways contribute a negligible amount to the observed stellar (halo) population at faint magnitudes, $g \gtrsim 17$.

5.2. Upper Limit on the Runaway Fraction

The runaway fraction of O- and B-type stars has long been known to be ∼40% and ∼5%, respectively (Blaauw 1961; Gies & Bolton 1986). However, there are few comparable

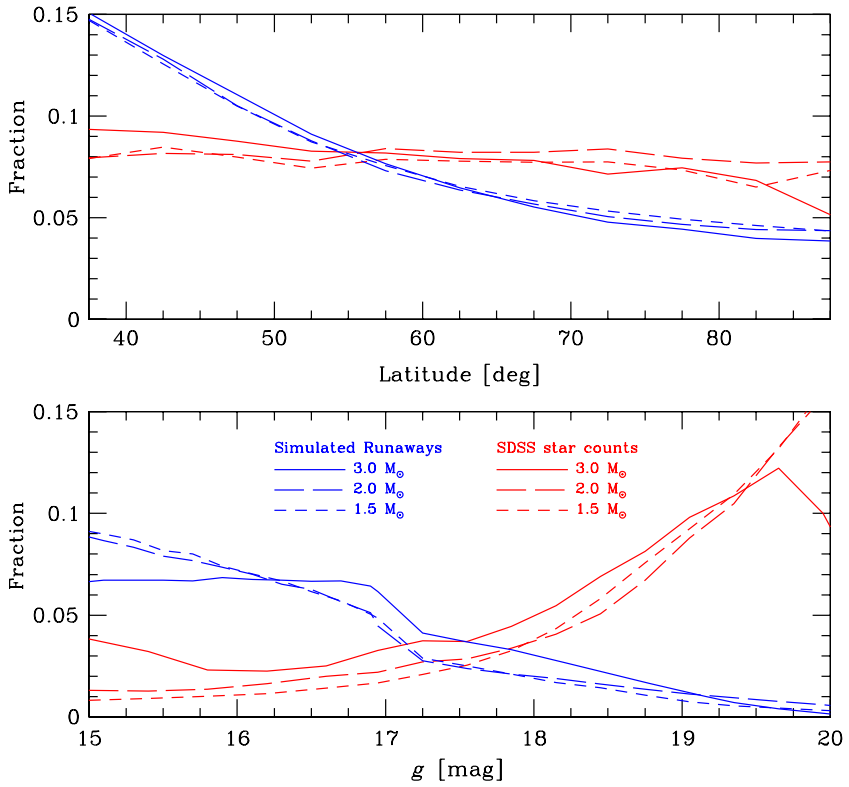

Figure 10. Comparison of the number fractions of simulated 1.5, 2, and 3 $M_{\odot}$ runaways in the SDSS survey region (blue lines) with SDSS star counts (red lines). Relative to the Galactic stellar population, runaways have the highest contrast at low latitudes and at bright magnitudes.

constraints on the fraction of A-type runaways. Stetson (1981) used tangential velocity cuts of bright stars with rough spectral types to estimate that at most ∼0.3% of solar neighborhood A-type stars are runaways. Here, we combine constraints from our simulations and existing spectroscopic surveys to place an independent upper limit on the fraction of 2 $M_{\odot}$ stars ejected as runaways.

To make this estimate, we use the Brown et al. (2008) spectroscopic survey of A-type stars in the 2MASS (Skrutskie et al. 2006). The Brown et al. (2008) survey is complete over 4300 deg^2 to a magnitude limit of $J_0 = 15.5$, equivalent to $g \simeq 15.5$ for a zero-color A star. Brown et al. (2008) find that 40% of A-type stars at 15th mag are main-sequence stars (the other 60% are evolved horizontal branch stars). A third of the main-sequence stars are consistent with having solar metallicity, thus 13% of 15th mag A stars are possible runaways. In our 2 $M_{\odot}$ simulation, however, the fraction of runaways is 6 times larger than the observed fraction in star counts at $g = 15$ (Figure 10). Thus, if the main-sequence A stars observed by Brown et al. (2008) are all runaways, the absolute fraction of A stars ejected as runaways is no larger than $0.13/6 \simeq 2\%$, in agreement with the upper limit estimated by Stetson (1981).

5.3. Runaways in the Inner Halo

We now broaden our discussion and look at the distribution of runaways in the context of the Galactic structure.

Spatially, 80% of runaways in our simulations are located at $|b| < 15^{\circ}$ (Figure 10), a population an observer might call "thick disk." The Galactic thick disk has an observed scale height of 0.75–1.0 kpc (i.e., Siegel et al. 2002; Girard et al. 2006; Jurić et al. 2008), and it dominates the number density of stars in the region 1 kpc $< |z| <$ 5 kpc. We note that claims of unusually large thick disk scale heights are possibly confused with the inner stellar halo (Kinman et al. 2009). By comparison, the number density of runaways in our simulations, selected with 7 kpc $< r_{\rm cyl} <$ 9 kpc and 1 kpc $< |z| <$ 5 kpc, is well fit by an exponential distribution with a vertical scale height $h_z = 0.54 \pm 0.01$ kpc.

Kinematically, runaways are a hot, rotating population analogous to the thick disk and inner stellar halo. In the region away from the plane $|b| > 15^{\circ}$, simulated runaways have a mean 135 km s^{-1} component of velocity in the direction of Galactic rotation, comparable to that observed for the thick disk (Chiba & Beers 2000). Runaways also have a 130 km s^{-1} heliocentric radial velocity dispersion, essentially identical to the velocity dispersion of inner halo stars with the same apparent magnitude. The Milky Way inner halo, as described by Carollo et al. (2007) and Morrison et al. (2009), has a small ∼25 km s^{-1} prograde rotation and a one-dimensional velocity dispersion of ∼120 km s^{-1}. Thus, runaways have similar kinematics to the Galactic thick disk and inner halo, and are difficult to identify by radial velocity alone.

The mean metallicity of the inner halo is [Fe/H]$= -1.6$ (Carollo et al. 2007), but Ivezić et al. (2008) report solar metallicity stars up to 5 kpc above the plane. Perhaps runaways can contribute to the high metallicity population and to the small prograde rotation observed in the inner stellar halo.

The inner halo is too metal poor to be composed entirely of runaways, yet metal-rich, short-lived runaways should be present in the halo of the Milky Way. The deaths of massive runaways must necessarily result in metal enrichment and energy input into the halo. This conclusion applies for all star-forming galaxies at all redshifts. In particular, runaways should be more abundant early in the evolution of a galaxy when the star formation rate is larger. Thus, the distribution of runaways may have important implications for feedback processes.

6. CONCLUSIONS

Runaway stars are an interesting class of objects because they connect star formation in the disk with the halo of the Milky Way. We explore these connections by using the Portegies Zwart (2000) distribution of binary-supernova ejections to inject stars into the Galactic potential. We track the progress of these stars from the Galactic disk to the Galactic halo and derive simulated catalogs of runaways.

We show that the velocity and spatial distributions of runaways depend on the Galactic potential and stellar lifetime. All runaways have a flattened spatial distribution, with higher velocity runaways at lower Galactic latitudes. Massive runaways do not live long enough to reach the outer halo. Thus, massive runaways are more concentrated toward the Galactic center and in the plane of the disk than low-mass runaways.

Kinematically, runaways are a hot, rotating population of stars with dynamical properties between the thick disk and the halo. In the solar neighborhood, runaways with masses of 1.5–3 $M_{\odot}$ have scale heights and rotation velocities comparable to the thick disk, and velocity dispersions comparable to the inner stellar halo. Although they do not have a unique signature in radial velocity surveys, runaways are overwhelmingly located at low Galactic latitudes and at bright apparent magnitudes. Our results suggest an upper limit of 2% of A-type stars ejected as runaways.

The kinematics of the unbound runaway HD 271791 provides an interesting comparison with the simulations. For runaways that reach distances of 60–100 kpc from the Galactic center, the simulations predict a peak in the initial distance of bound (unbound) stars at 7–12 kpc (10–15 kpc). Heber et al. (2008) conclude that HD 271791 originated from 12 kpc $\lesssim r \lesssim$ 16 kpc (Heber et al. 2008). Clear tests of the simulations require larger samples of runaways with high-quality proper motions and good estimates for their starting locations in the disk.

Radial velocity surveys for high-velocity outliers are unlikely to confuse runaway stars with HVSs. Among ejected stars with velocities exceeding 400 km s^{-1}, runaways (1) are brighter ($g \lesssim 18$), (2) have smaller velocities ($v \lesssim 450$ km s^{-1}), and (3) are more concentrated to lower galactic latitudes ($b \lesssim 35^{\circ}$) than HVS with typical $g \gtrsim 18$, $v \approx$ 400–700 km s^{-1}, and random b in the range $30^{\circ} < b < 90^{\circ}$. We estimate that at most ∼one runaway contaminates the Brown et al. sample of HVSs.

Future progress on the theory of runaways requires predictions for the velocity distribution from the dynamical ejection mechanism. Although this process can yield higher ejection velocities than the binary-supernova ejection mechanism, uncertainties in the stellar merger rate during close encounters complicate calculations of a realistic maximum ejection velocity and a distribution of ejection velocities.

For both mechanisms, better estimates of predicted rates are needed to constrain predictions for the frequency and kinematics of runaways. Extending the Portegies Zwart (2000) simulations to lower mass stars would improve our estimate for the rate of runaways from the binary-supernova ejection mechanism among A-type stars. Simulations of ensembles of dense star clusters would yield ejections rates for the dynamical ejection mechanism.

Measurements of proper motions and metallicities of inner halo stars can also improve our understanding of runaways. Identifying the fraction of halo stars with roughly solar metallicity can yield a better estimate of the frequency of runaways. Proper motions and radial velocities place clear constraints on the origin of runaways for comparison with theoretical simulations.

We acknowledge Elliott Barcikowsky's contribution to the early stages of this work. Comments from an anonymous referee greatly improved our presentation. This research makes use of NASA's Astrophysics Data System Bibliographic Services and data products from the Sloan Digital Sky Survey, which was funded by the Alfred P. Sloan Foundation and Participating Institutions. This work was supported in part by the Smithsonian Institution.

REFERENCES

Abadi, M. G., Navarro, J. F., & Steinmetz, M. 2009, ApJ, 691, L63
Adelman-McCarthy, J. K., et al. 2008, ApJS, 175, 297
Blaauw, A. 1961, Bull. Astron. Inst. Netherlands, 15, 265
Blaauw, A., & Morgan, W. W. 1954, ApJ, 119, 625
Brand, J., & Wouterloot, J. G. A. 2007, A&A, 464, 909
Bromley, B. C., & Kenyon, S. J. 2006, AJ, 131, 2737
Bromley, B. C., Kenyon, S. J., Geller, M. J., Barcikowski, E., Brown, W. R., & Kurtz, M. J. 2006, ApJ, 653, 1194
Brown, W. R., Beers, T. C., Wilhelm, R., Allende Prieto, C., Geller, M. J., Kenyon, S. J., & Kurtz, M. J. 2008, AJ, 135, 564
Brown, W. R., Geller, M. J., & Kenyon, S. J. 2009a, ApJ, 690, 1639
Brown, W. R., Geller, M. J., Kenyon, S. J., & Bromley, B. C. 2009b, ApJ, 690, L69
Brown, W. R., Geller, M. J., Kenyon, S. J., & Kurtz, M. J. 2005, ApJ, 622, L33
Brown, W. R., Geller, M. J., Kenyon, S. J., & Kurtz, M. J. 2006a, ApJ, 640, L35
Brown, W. R., Geller, M. J., Kenyon, S. J., & Kurtz, M. J. 2006b, ApJ, 647, 303
Brown, W. R., Geller, M. J., Kenyon, S. J., Kurtz, M. J., & Bromley, B. C. 2007a, ApJ, 660, 311
Brown, W. R., Geller, M. J., Kenyon, S. J., Kurtz, M. J., & Bromley, B. C. 2007b, ApJ, 671, 1708
Burrows, A., Hayes, J., & Fryxell, B. A. 1995, ApJ, 450, 830
Carollo, D., et al. 2007, Nature, 450, 1020
Chiba, M., & Beers, T. C. 2000, AJ, 119, 2843
Conlon, E. S., Dufton, P. L., Keenan, F. P., & Leonard, P. J. T. 1990, A&A, 236, 357
Davies, M. B., King, A., & Ritter, H. 2002, MNRAS, 333, 463
Demarque, P., Woo, J.-H., Kim, Y.-C., & Yi, S. K. 2004, ApJS, 155, 667
de Wit, W. J., Testi, L., Palla, F., & Zinnecker, H. 2005, A&A, 437, 247
Diehl, R., et al. 2006, Nature, 439, 45
Dray, L. M., Dale, J. E., Beer, M. E., Napiwotzki, R., & King, A. R. 2005, MNRAS, 364, 59
Edelmann, H., Napiwotzki, R., Heber, U., Christlieb, N., & Reimers, D. 2005, ApJ, 634, L181
Fregeau, J. M., Cheung, P., Portegies Zwart, S. F., & Rasio, F. A. 2004, MNRAS, 352, 1
Fuentes, C. I., Stanek, K. Z., Gaudi, B. S., McLeod, B. A., Bogdanov, S., Hartman, J. D., Hickox, R. C., & Holman, M. J. 2006, ApJ, 636, L37
Gies, D. R. 1987, ApJS, 64, 545
Gies, D. R., & Bolton, C. T. 1986, ApJS, 61, 419
Girard, T. M., Korchagin, V. I., Casetti-Dinescu, D. I., van Altena, W. F., López, C. E., & Monet, D. G. 2006, AJ, 132, 1768
Girardi, L., Bertelli, G., Bressan, A., Chiosi, C., Groenewegen, M. A. T., Marigo, P., Salasnich, B., & Weiss, A. 2002, A&A, 391, 195
Girardi, L., Grebel, E. K., Odenkirchen, M., & Chiosi, C. 2004, A&A, 422, 205
Greenstein, J. L. 1957, AJ, 62, 16
Greenstein, J. L., & Sargent, A. I. 1974, ApJS, 28, 157
Gvaramadze, V. V. 2009, MNRAS, 395, L85
Hansen, B. M. S., & Milosavljević, M. 2003, ApJ, 593, L77
Heber, U., Edelmann, H., Napiwotzki, R., Altmann, M., & Scholz, R.-D. 2008, A&A, 483, L21
Helmi, A. 2008, A&AR, 15, 145
Hills, J. G. 1983, ApJ, 267, 322
Hills, J. G. 1988, Nature, 331, 687
Hirsch, H. A., Heber, U., O'Toole, S. J., & Bresolin, F. 2005, A&A, 444, L61
Hogg, D. W., Blanton, M. R., Roweis, S. T., & Johnston, K. V. 2005, ApJ, 629, 268
Holmgren, D. E., McCausland, R. J. H., Dufton, P. L., Keenan, F. P., & Kilkenny, D. 1992, MNRAS, 258, 521
Hoogerwerf, R., de Bruijne, J. H. J., & de Zeeuw, P. T. 2001, A&A, 365, 49
Hoffer, J. B. 1983, AJ, 88, 1420
Hut, P., & Bahcall, J. N. 1983, ApJ, 268, 319

Humason, M. L., & Zwicky, F. 1947, ApJ, 105, 85
Ibata, R. A., Gilmore, G., & Irwin, M. J. 1994, Nature, 370, 194
Ivezić, Ž., et al. 2008, ApJ, 684, 287
Jurić, M., et al. 2008, ApJ, 673, 864
Justham, S., Wolf, C., Podsiadlowski, P., & Han, Z. 2009, A&A, 493, 1081
Kenyon, S. J., Bromley, B. C., Geller, M. J., & Brown, W. R. 2008, ApJ, 680, 312
Kilkenny, D., & Muller, S. 1989, South Afr. Astron. Obs. Circ., 13, 69
Kilkenny, D., & Stone, L. E. 1988, MNRAS, 234, 1011
Kinman, T. D., Morrison, H. L., & Brown, W. R. 2009, AJ, 137, 3198
Kobulnicky, H. A., & Fryer, C. L. 2007, ApJ, 670, 747
Kollmeier, J. A., & Gould, A. 2007, ApJ, 664, 343
Leonard, P. J. T. 1991, AJ, 101, 562
Leonard, P. J. T. 1993, in ASP Conf. Ser. 45, Luminous High-Latitude Stars, ed. D. Sasselov (San Francisco, CA: ASP), 360
Leonard, P. J. T., & Duncan, M. J. 1988, AJ, 96, 222
Leonard, P. J. T., & Duncan, M. J. 1990, AJ, 99, 608
López-Morales, M., & Bonanos, A. Z. 2008, ApJ, 685, L47
Lynn, B. B., Keenan, F. P., Dufton, P. L., Saffer, R. A., Rolleston, W. R. J., & Smoker, J. V. 2004, MNRAS, 349, 821
Magee, H. R. M., Dufton, P. L., Keenan, F. P., Rolleston, W. R. J., Kilkenny, D., O'Donoghue, D., Koen, C., & Stobie, R. S. 2001, MNRAS, 324, 747
Martin, J. C. 2004, AJ, 128, 2474
Martin, J. C. 2006, AJ, 131, 3047
Mitchell, K. J., Saffer, R. A., Howell, S. B., & Brown, T. M. 1998, MNRAS, 295, 225
Morrison, H. L., et al. 2009, ApJ, 694, 130
Murphy, J. W., Burrows, A., & Heger, A. 2004, ApJ, 615, 460
O'Leary, R., & Loeb, A. 2008, MNRAS, 383, 86
Portegies Zwart, S. F. 2000, ApJ, 544, 437
Poveda, A., Ruiz, J., & Allen, C. 1967, Bol. Obs. Tonantzintla Tacubaya, 4, 860
Press, W. H., Flannery, B. P., Teukolsky, S. A., & Vetterling, W. T. 1992, Numerical Recipes: The Art of Scientific Computing (Cambridge: Cambridge Univ. Press)
Przybilla, N., Nieva, M. F., Heber, U., & Butler, K. 2008a, ApJ, 684, L103
Przybilla, N., Nieva, M. F., Tillich, A., Heber, U., Butler, K., & Brown, W. R. 2008b, A&A, 488, L51
Ramspeck, M., Heber, U., & Moehler, S. 2001, A&A, 378, 907
Rolleston, W. R. J., Hambly, N. C., Keenan, F. P., Dufton, P. L., & Saffer, R. A. 1999, A&A, 347, 69
Salpeter, E. E. 1955, ApJ, 121, 161
Schaerer, D., Charbonnel, C., Meynet, G., Maeder, A., & Schaller, G. 1993, A&AS, 102, 339
Schaller, G., Schaerer, D., Meynet, G., & Maeder, A. 1992, A&AS, 96, 269
Siebert, A., et al. 2008, MNRAS, 391, 793
Siegel, M. H., Majewski, S. R., Reid, I. N., & Thompson, I. B. 2002, ApJ, 578, 151
Skrutskie, M. F., et al. 2006, AJ, 131, 1163
Smith, M. C., et al. 2007, MNRAS, 379, 755
Stetson, P. B. 1981, AJ, 86, 1882
Stone, R. C. 1991, AJ, 102, 333
Xue, X., et al. 2008, ApJ, 684, 1143
Yu, Q., & Tremaine, S. 2003, ApJ, 599, 1129
Zwitter, T., et al. 2008, AJ, 136, 421